HYBRID ATOMISTIC-CONTINUUM APPROACH TO DESCRIBE INTERFACIAL PROPERTIES BETWEEN IMMISCIBLE LIQUIDS

K. M. Issa*,[1], and P. Poesio*,[2]

*Università degli Studi di Brescia, via Branze 38, 25123, Brescia Italy
email:khaled.mo.issa@gmail.com[1], pietro.poesio@ing.unibs.it[2]

ABSTRACT

The study of immiscible liquid-liquid interfaces (LLIs) is of importance in many phenomena in engineering, chemical, and biological systems. At an immiscible LLI, a slip occurs as a result of poor mixing, and relatively weaker atomic interactions between the two liquids. One of the main difficulties in modeling immiscible (and partially miscible) LLIs is the assignment of boundary conditions at the interface. In continuum-based modeling of macroscale systems, a no-slip boundary condition is generally assumed at the LLI. The issue of interfacial slip, however, becomes especially relevant for micro-, and nanofluidics where interface dynamics play a key role, and the slip magnitude can strongly affect the flow behavior. In that respect, molecular dynamics (MD) is a vital tool for modeling LLIs at the atomic scale. In this paper, we present a hybrid atomistic-continuum (HAC) approach that utilizes MD at the LLI to directly extract boundary conditions needed by a continuum solver. Our focus is on the treatment of the atomistic subdomain (Ω_A), specifically when it comes to the proper termination of Ω_A, and the coupling to an external continuum field. The model is tested using a Couette flow under varying flow speeds. Finally, we demonstrate the ability of the model to accurately predict the slip coefficient at the LLI.

INTRODUCTION

Liquid-Liquid Interfaces (LLIs), formed by two immiscible liquids, occur in a wide range of systems. For instance, in biology, interfaces between two immiscible liquid electrolyte solutions are of great importance as they occur in tissues and cells of all living organisms. In oil and gas industry, the balance between break-up and coalescence (both interfacial phenomena) determine the occurrence of phase inversion, a process that can lead to the blockage of the entire pipeline with a huge economical impact. Furthermore, in recent lab-on-a-chip technology, liquid droplets, moving through an immiscible liquid, are used as chemical (and biological) reactors, where reactions are carried out while the droplet is transported along micro-channels. Hence, the proper understanding, and modeling of LLI dynamics is of great significance to many industries.

The slip behavior at immiscible LLIs is a nanoscale phenomenon, and requires atomic resolution to accurately capture the relevant physics. Continuum methods generally assume a no-slip boundary condition at the LLI, which could provide reasonable accuracy on a macroscale level. This approximation loses validity at the micro- and nanoscale, due to the relatively higher surface-to-volume ratio. Additionally, the amount of slip at such scales can be comparable to the characteristic length of the system and therefore should be carefully accounted for.

Continuum theory, in the form of the Navier-Stokes (NS) equations, can accurately predict flow dynamics in the regions far removed from LLI effects. On the other hand, molecular dynamics (MD) is capable of capturing important nanoscale physics at the LLI [1, 2, 3, 4]. The method is, however, computationally demanding and modeling is presently limited to systems within the nanoscale. Hybrid atomistic-continuum (HAC) modeling can alleviate these shortcomings by decomposing the domain into a continuum description (Ω_{C}) and an atomistic one (Ω_{A}). By limiting Ω_{A} to the LLI, boundary conditions for the NS solution at the interface are naturally recovered through MD. With this domain-decomposition approach, the two descriptions partially overlap in a region ($\Omega_{\mathrm{C}\to\mathrm{A}}$+ $\Omega_{\mathrm{A}\to\mathrm{C}}$) where information is exchanged [5]. The accuracy of the method relies on the proper application of continuum state variables onto Ω_{A}, and the consistency of transport coefficients between the two descriptions.

In this paper, we present a one-way coupling algorithm for the HAC modeling of one-dimensional LLIs. The focus is on the proper termination of Ω_{A} and on the imposition of boundary conditions of the form $\Omega_{\mathrm{C}\to\mathrm{A}}$. The boundaries of Ω_{A} are modeled as reflective walls supplemented with an adaptive boundary force, to prevent artificial density layering. The method is tested using a Couette flow with different velocities. The velocity profiles at the LLI are compared with the continuum NS solution. The predicted viscosity, and slip coefficients are shown to agree well with the literature.

METHODOLOGY

Particles in the atomistic subdomain (Ω_{A}) interact via the Lennard-Jones (LJ) potential:

$$U_{\mathrm{LJ}}(r_{ij}) = 4\varepsilon\left[\left(\frac{\sigma}{r_{ij}}\right)^{12} - \beta\left(\frac{\sigma}{r_{ij}}\right)^{6}\right] \qquad (1)$$

where r_{ij} is the separation distance between particles i, and j. The energy, and length scales are taken to be those of argon: $\varepsilon = 0.996$ kJmol^{-1}, and $\sigma = 3.4$ Å (1 Å $= 10^{-10}$m). The potential is force-shifted [6] and a cutoff radius of $r_{\mathrm{c}} = 3\sigma = 10.2$Å is employed. The parameter β is used to tune the attractive part of the potential between the two liquids (L_1, and L_2). To induce

complete immiscibility, we assign $\beta_{11} = \beta_{22} = 1.0$ and $\beta_{12} = 0.0$. The position ($\mathbf{r}_i$) and velocity ($\mathbf{v}_i$) vectors of each particle i are governed by Newton's equation of motion:

$$\frac{d\mathbf{r}_i}{dt} = \mathbf{v}_i \tag{2}$$

$$\frac{d\mathbf{v}_i}{dt} = \frac{\mathbf{F}_i}{m_i} \tag{3}$$

where $\mathbf{F}_i = -\sum_{j\neq i} \nabla_{\mathbf{r}_{ij}} U_{\mathrm{LJ}}$ is the total force acting on particle i, with mass $m_i = 40$ gmol^{-1}. Eqs. (2)-(3) are solved using the leap-frog algorithm:

$$\mathbf{v}_i^{n+1/2} = \mathbf{v}_i^{n-1/2} + \delta t\ \mathbf{F}_i^n / m_i \tag{4}$$

$$\mathbf{r}_i^{n+1} = \mathbf{r}_i^n + \delta t\ \mathbf{v}_i^{n+1/2} \tag{5}$$

where δt is the time step. Superscripts in Eqs. (4)-(5) denote the relative time level of each variable.

The atomistic subdomain Ω_A describing the LLI is shown in Fig. 1. The system dimensions are: $L_x \times L_y \times L_z = 14.2\sigma \times 13.6\sigma \times 6.8\sigma$. The size is chosen to give a bulk liquid density of $\rho = 1369$kgm^{-3} ($\rho^* = \rho\sigma^3 N_{\mathrm{av}} m^{-1} = 0.81$), with a total of $N = 1024$ particles. Periodic boundary conditions are used along the y- and z-axes. In the x-direction, the system is terminated using a reflective wall and an adaptive boundary force (details below). Velocity and temperature measurements are recorded in bins of size $\delta x = 0.79\sigma$ along the x-axis. To capture the LLI, a higher bin resolution of $\delta x_\rho = 0.1\delta x$ is used for the density profiles. The system is equilibrated at $T = 132$K ($T^* = k_b T/\varepsilon = 1.1$), using a Berendsen thermostat [7] with a time constant of 0.5 ps (1 ps $= 10^{-12}$s). A time step of $\delta t = 5$fs (1 fs $= 10^{-15}$s, $\delta t^* = 0.0023\tilde{t}$, $\tilde{t} = \sigma\, m^{0.5}\varepsilon^{-0.5}$) is used with total runs of 15 ns duration.

Particles that attempt to leave Ω_{A} along the non-periodic x-axis are specularly reflected back into Ω_{A} by reversing the velocity component normal to that plane (v_x). This guarantees a constant number of particles (N) in Ω_{A}, however, it does not account for the lack of periodicity along that direction. Thus, causing artificial density layering normal to the reflective boundary. One way to alleviate this issue is to supplement the reflections with a boundary force that 'mimics' on average the forces felt by a particle in a periodic system [8]. The boundary force in [8] was derived by measurement in a periodic system and applied as a function of distance to the reflective boundary. For supercritical conditions, this was found to significantly reduce the artificial layering. However, the performance of this technique was shown to deteriorate at higher densities, and/or lower temperatures, conditions which are relevant for LLI analysis. This drawback was overcome by extracting the boundary force using a control algorithm [9, 10], which we employ in our model. First, the density in each bin is averaged in time intervals of 5 ps. The noise in the density profile is then reduced by passing it twice through a Gaussian filter as follows (see appendix A for details):

$$\rho_1(x) = \phi^{-1} \int \rho(x) \exp\left[-(x-x_1)^2/\phi^2\right] dx_1 \tag{6}$$

$$\rho_2(x) = \phi^{-1} \int \rho_1(x) \exp\left[-(x-x_2)^2/\phi^2\right] dx_2 \tag{7}$$

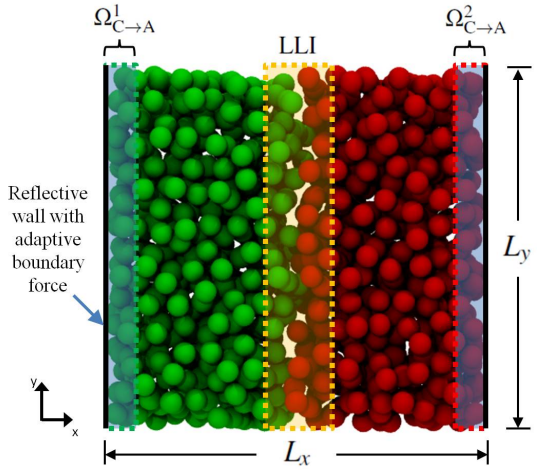

Figure 1. Atomistic liquid ($L_1 + L_2$) subdomain (Ω_{A}) at the LLI. External field quantities are applied within the shaded regions denoted by $\Omega^j_{\mathrm{C}\to\mathrm{A}}$ ($j = 1, 2$).

where: ρ_1 and ρ_2 are the density profiles subsequent to the first and second Gaussian smoothing, respectively. The integrals are evaluated discretely with a cutoff of $3\delta x_\rho$, and $\phi = 2\delta x_\rho$. The gradient of the density profile $\nabla\rho_2(x)$ is then used as a correction mechanism to adapt the boundary force F_b which is initially at zero:

$$F_b(x, t + t_{ad}) = F_b(x,t) - \nabla\rho_2\sqrt{\lambda} \tag{8}$$

where t_{ad} is the 5 ps averaging period. The parameter λ is used to enact corrections faster away from the boundary which helps prevent the forces close to the boundary from over-shooting. In this study, we select $\lambda = 1.1 \times 10^{-4} q$, where q is the bin number counted from the boundary for each liquid, respectively.

The system is first thermostatted for 50 ps, with reflective boundaries only. The adaptation of F_b commences following the equilibration period. Additionally, the application of boundary conditions to the particles in $\Omega^j_{\mathrm{C}\to\mathrm{A}}$ ($j = 1, 2$) is carried out simultaneously. For the purpose of studying LLI dynamics in the presence of a Couette flow, we apply opposing velocities of $u^*_C = \pm$ 0.2, 0.4, 0.6, and 0.8, along the y-axis. The velocity u^*_C is ramped up to its target value over a period of 50 ps. For each liquid, u^*_C is enforced by applying an additional body force $F_{u_{\mathrm{C}}}$ in the y-direction to each atom within $\Omega^j_{\mathrm{C}\to\mathrm{A}}$ ($j = 1, 2$), as given by (see Appendix B):

$$F_{u_{\mathrm{C}}} = \frac{m}{\delta t}\left(u_C - v_{\mathrm{com_y}}\right) - \frac{F_{\mathrm{com_y}}}{N_{\Omega^j_{\mathrm{C}\to\mathrm{A}}}} \tag{9}$$

$$v_{\mathrm{com_y}} = \frac{1}{N_{\Omega^j_{\mathrm{C}\to\mathrm{A}}}} \sum_{i=1}^{N_{\Omega^j_{\mathrm{C}\to\mathrm{A}}}} v_{y,i} \tag{10}$$

where $v_{\mathrm{com_y}}$ is the center-of-mass y-velocity of particles in $\Omega^j_{\mathrm{C}\to\mathrm{A}}$ ($j = 1, 2$), and $F_{\mathrm{com_y}}$ is the corresponding net force. Furthermore, the temperature is maintained at $T^*_C = 1.1$ via direct velocity scaling about the center-of-mass velocity:

$$\mathbf{v}_i = \left(\mathbf{v}_i - \mathbf{u}_{\Omega^j_{\mathrm{C}\to\mathrm{A}}}\right)\sqrt{\frac{T_C}{T_{\Omega^j_{\mathrm{C}\to\mathrm{A}}}}} + \mathbf{u}_{\Omega^j_{\mathrm{C}\to\mathrm{A}}} \tag{11}$$

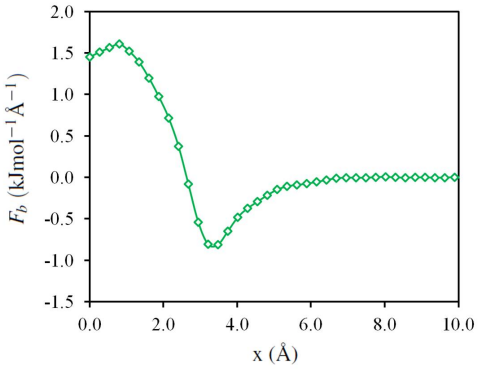

Figure 2. Adaptive boundary force (F_b) for L_1 with $u_C^* = 0.2$. Distance measured from the reflective boundary of $\Omega^1_{C\to A}$.

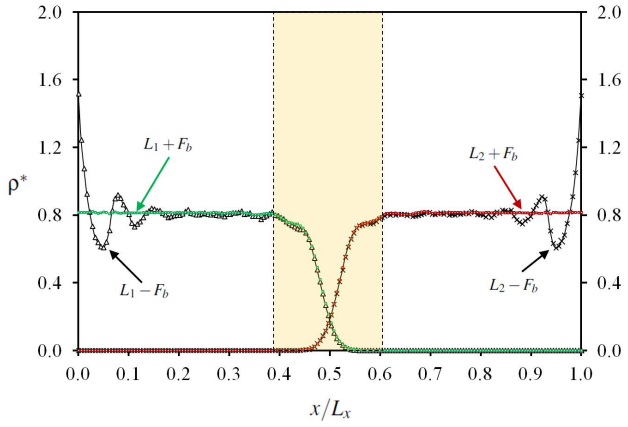

Figure 3. Density profiles for $u_C^* = 0.2$, with (+) and without (-) the action of F_b. The shaded region marks the depleted zone at the LLI.

where $\left\langle \mathbf{u}_{\Omega^j_{C\to A}} \right\rangle = [0, u_C, 0]$ for $j = 1$, and $[0, -u_C, 0]$ for $j = 2$. The variable $T_{\Omega^j_{C\to A}}$ is the instantaneous temperature of particles in $\Omega^j_{C\to A}$ $(j = 1, 2)$.

RESULTS & DISCUSSION

Data sampling was started after 5 ns, for which the boundary force, and velocity profiles exhibited steady-state behavior. The collection of data was carried out for an additional 10 ns. The adaptive boundary force (F_b) for $u_C^* = 0.2$ is shown in Fig. 2. Close to the boundary, F_b is repulsive in nature, with an attractive component further away. The effectiveness of F_b in eliminating the density layering at the boundary is shown in Fig 3. A uniform density of $\rho^* = 0.81$ can be seen away from the depleted region at the LLI between the two immiscible liquids.

The steady-state velocity profile for $u_C^* = \pm 0.4$ is shown in Fig. 4, along with the analytical solution for a Couette flow ($d^2u/dx^2 = 0$). Using the imposed velocities in $\Omega^j_{C\to A}$ $(j = 1, 2)$ as boundary conditions, the resulting analytical velocity profile is given by:

$$u(x) = -\frac{2u_C}{L_x}x + u_C \tag{12}$$

When normalized by u_C, all other cases exhibited a similar trend. The deviation from the analytical solution increases closer to the LLI, as a result of the interfacial slip. To validate

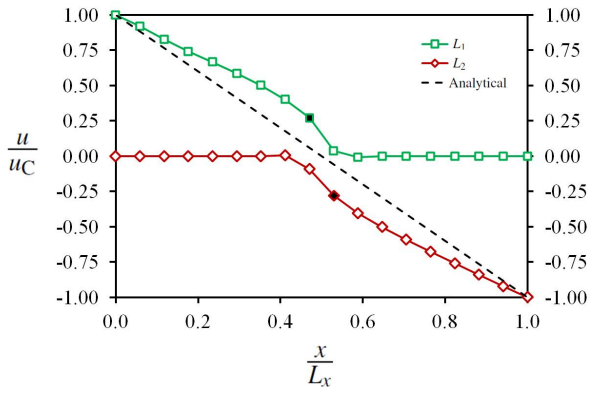

Figure 4. Velocity profile across the LLI for $u_C^* = \pm 0.4$, and the analytical solution given by Eq. (12). Shaded data points are used to measure apparent slip (δu).

Table 1. All values are in reduced units. Where appropriate, results are listed in the form $L_1(L_2)$.

u_C^*	$\frac{du}{dx}$ $(\times 10^2)$	τ^* $(\times 10^2)$	η^*	δu^*	α
0.2	2.10 (2.11)	4.47 (4.46)	2.13 (2.12)	0.115	2.56
0.4	4.23 (4.20)	9.20 (9.20)	2.17 (2.19)	0.220	2.39
0.6	6.33 (6.38)	13.9 (13.9)	2.20 (2.18)	0.326	2.36
0.8	8.69 (8.66)	18.2 (18.3)	2.13 (2.14)	0.522	2.83

the velocity profiles, we first compare the viscosity of the liquids to that measured using equilibrium MD [11], at a representative state point of $\rho^* = 0.81$, and $T^* = 1.1$. This is carried out by calculating the average amount of momentum (Δp) added every time step in $\Omega^j_{C\to A}$ $(j = 1, 2)$ to maintain the flow. Using Δp, the shear stress (τ), or momentum flux, is estimated using:

$$\tau = \frac{\Delta p}{\delta t A} \tag{13}$$

where $A = L_y \times L_z$ is the cross-sectional area parallel to the flow. The viscosity is then computed from: $\eta = \tau(du/dx)^{-1}$. The calculation of the velocity gradient (du/dx) from the velocity profiles (similar to Fig. 4) is limited to the linear region $(x/L_x \approx 0.3)$ away from the depleted zone. The viscosity values are given in Table 1, and are in good agreement with the value of $\eta^*_{ref} = 2.18$ obtained from [11]. Furthermore, we compare the slip coefficient (α) predicted using our model with that reported for immiscible LJ liquids $\alpha_{ref_{average}} = 2.53$ [1]. Using the velocity jump at the LLI, and the measured shear stress τ, the slip coefficient is estimated by:

$$\alpha = \frac{\delta u}{\tau} \tag{14}$$

where δu is the apparent slip, and is measured using the data points indicated in Fig. 4. As can be seen in Table 1, the slip coefficient is accurately predicted within Ω_A.

CONCLUSION

We have presented an HAC algorithm for imposing continuum field variables onto an atomistic subdomain (Ω_A) for the purpose of studying slip at immiscible LLIs. Density layering at the interface between the two descriptions was eliminated by the use of an adaptive boundary force. The momentum flux applied and the resulting velocity gradient in the linear zone produce a viscosity that is in close agreement with that reported in the literature. The method is also shown to accurately capture the slip coefficient (α) at the LLI. Our plans include the implementation of this algorithm with two-way coupling to the continuum description (Ω_C).

NOMENCLATURE

N_{av} Avogadro's number
k_b Boltzmann constant [$m^2 kgs^{-2} K^{-1}$]

REFERENCES

[1] J. Koplik, and J. R. Banavar, Slip, immiscibility, and boundary conditions at the liquid-liquid interface, *Phys. Rev. Lett.,* vol. 96, pp. 0445051-0445054,2006.

[2] Y. Hu, X. Zhang, and W. Wang, Boundary conditions at the liquid-liquid interface in the presence of surfactants, *Langmuir,* vol. 26, pp. 10693-10702,2010.

[3] G. Galliero, Lennard-Jones fluid-fluid interfaces under shear, *Phys. Rev. E,* vol. 81, pp. 0563061-0563067,2010.

[4] Q. Ehlinger, L. Joly, and O. Pierre-Louis, Giant slip at liquid-liquid interfaces using hydrophobic ball bearings, *Phys. Rev. Lett.,* vol. 110, pp. 1045041-1045045,2013.

[5] K. M. Mohamed, and A. A. Mohamad, A review of the development of hybrid atomistic-continuum methods for dense fluids, *Microfluid. Nanofluid.,* vol. 8, pp. 283-302,2010.

[6] M. P. Allen and D. J. Tildesley, *Computer simulation of liquids*, Oxford University Press, New York, 1987.

[7] H. J. C. Berendsen, J. P. M. Postma, W. F. van Gunsteren, A. DiNola, and J. R. Haak, Molecular dynamics with coupling to an external bath, *J. Chem. Phys.,* vol. 81, pp. 3684-3690,1984.

[8] T. Werder, J. H. Walther, and P. Koumoutsakos, Hybrid atomistic-continuum method for the simulation of dense fluid flows, *J. Comput. Phys.,* vol. 205, pp. 373-390,2005.

[9] E. M. Kotsalis, J. H. Walther, and P. Koumoutsakos, Control of density fluctuations in atomistic-continuum simulations of dense liquids, *Phys. Rev. E,* vol. 76, pp. 0167091-0167097,2007.

[10] E. M. Kotsalis, J. H. Walther, E. Kaxiras, and P. Koumoutsakos, Control algorithm for multiscale flow simulations of water, *Phys. Rev. E,* vol. 79, pp. 0457011-0457014,2009.

[11] R. L. Rowley, and M. M. Painter, Diffusion and viscosity equations of state for a Lennard-Jones fluid obtained from molecular dynamics simulations, *Int. J. Thermophys.,* vol. 18, pp. 1109-1121,1997.

Appendix A: Discrete Gaussian filter equations

For clarity, the density bin spacing is labeled δx instead of δx_ρ. In discrete form, the Gaussian filer of Eq. (6) with a cutoff of $3\delta x$ is given by:

$$\rho_1(x) = \phi^{-1} \sum_{x_1=x-3\delta x}^{x+3\delta x} \rho(x_1) e^{-\frac{(x-x_1)^2}{\phi^2}} \delta x \tag{15}$$

which expands to:

$$\rho_1(x) = \phi^{-1} \Big[\rho(x-3\delta x)\, e^{-\left(\frac{3\delta x}{\phi}\right)^2} + \rho(x-2\delta x)\, e^{-\left(\frac{2\delta x}{\phi}\right)^2} + \rho(x-\delta x)\, e^{-\left(\frac{\delta x}{\phi}\right)^2} + \rho(x) + \rho(x+\delta x)\, e^{-\left(\frac{\delta x}{\phi}\right)^2} + \rho(x+2\delta x)\, e^{-\left(\frac{2\delta x}{\phi}\right)^2} + \rho(x+3\delta x)\, e^{-\left(\frac{3\delta x}{\phi}\right)^2} \Big] \delta x$$

using $\phi = 2\ \delta x$:

$$\rho_1(x) = \frac{1}{2} \Big[\rho(x-3\delta x)\, e^{-\left(\frac{3}{2}\right)^2} + \rho(x-2\delta x)\, e^{-(1)^2} + \rho(x-\delta x)\, e^{-\left(\frac{1}{2}\right)^2} + \rho(x) + \rho(x+\delta x)\, e^{-\left(\frac{1}{2}\right)^2} + \rho(x+2\delta x)\, e^{-(1)^2} + \rho(x+3\delta x)\, e^{-\left(\frac{3}{2}\right)^2} \Big]$$

Normalizing by half the sum of the density coefficients: $\frac{1}{2}\left[2e^{-\left(\frac{3}{2}\right)^2} + 2e^{-(1)^2} + 2e^{-\left(\frac{1}{2}\right)^2} + 1\right] = 1.75208$, produces the final discrete equation:

$$\rho_1^i = 0.0301\rho^{i\pm3} + 0.1050\rho^{i\pm2} + 0.2223\rho^{i\pm1} + 0.2854\rho^i \tag{16}$$

where i refers to the bin number. Equation (16) is suitable for bins with at least three neighbors on either side. That is, for $i = 4$ to $N_{\text{bin}} - 3$. For the rest of the bins, the contribution to the smoothed value depends on the maximum number of neighboring bins on either side. The derivation is similar to the above, and can be shown to produce the following complete set:

$$\begin{aligned}
&\rho_1^i = \rho^i && i = 1, \text{or } N_{\text{bin}} \\
&\rho_1^i = 0.3045\rho^{i\pm1} + 0.3910\rho^i && i = 2, \text{or } N_{\text{bin}} - 1 \\
&\rho_1^i = 0.1117\rho^{i\pm2} + 0.2365\rho^{i\pm1} + 0.3036\rho^i && i = 3, \text{or } N_{\text{bin}} - 2 \\
&\rho_1^i = 0.0301\rho^{i\pm3} + 0.1050\rho^{i\pm2} + 0.2223\rho^{i\pm1} + 0.2854\rho^i && i = 4 \text{ to } N_{\text{bin}} - 3
\end{aligned}$$

where i denotes the bin number.

Appendix B: Derivation of flow driving body force (F_{u_C})

The following derivation is based on the leap-frog algorithm Eqs. (4)-(5). For a system of N particles, the center of mass velocity along any one dimension is given by:

$$v_{\text{com}}^{n-\frac{1}{2}} = \frac{1}{N} \sum_{i=1}^{N} v_i^{n-\frac{1}{2}} \tag{17}$$

If the *total* force at step n is: $F_{\text{com}}^n = \sum_{i=1}^{N} F_i^n$, then we seek an additional body force $F_{u_C}^n$ to be applied uniformly to each

particle in order to drive the flow with a velocity u_{C}. By setting $v_{\mathrm{com}}^{n+\frac{1}{2}} = u_{\mathrm{C}}$:

$$u_{\mathrm{C}} = v_{\mathrm{com}}^{n-\frac{1}{2}} + \frac{\delta t}{Nm} F_{\mathrm{com}}^{n} + \frac{\delta t}{Nm} \sum_{i=1}^{N} F_{u_{\mathrm{C}}}^{n} \tag{18}$$

where Nm is the total mass of the system. Solving for the *total* body force gives:

$$\sum_{i=1}^{N} F_{u_{\mathrm{C}}}^{n} = \frac{Nm}{\delta t} \left(u_{\mathrm{C}} - v_{\mathrm{com}}^{n-\frac{1}{2}} \right) - F_{\mathrm{com}}^{n} \tag{19}$$

when applied uniformly to each particle, that translates to:

$$F_{u_{\mathrm{C}}}^{n} = \frac{m}{\delta t} \left(u_{\mathrm{C}} - v_{\mathrm{com}}^{n-\frac{1}{2}} \right) - \frac{F_{\mathrm{com}}^{n}}{N} \tag{20}$$